BCS-BEC crossover and effects of density fluctuations in a two-component Fermi gas described by the three-dimensional attractive Hubbard model

H. Tamaki,[1] Y. Ohashi,[2,3] and K. Miyake[1]
[1]*Department of Materials Engineering Science, Graduate School of Engineering Science, Osaka University, Toyonaka, Osaka 560-8531, Japan*
[2]*Faculty of Science and Technology, Keio University, Hiyoshi, Yokohama 223-8522, Japan*
[3]*CREST (JST), 4-1-8 Honcho, Saitama 332-0012, Japan*
(Received 14 March 2008; published 18 June 2008)

We investigate the superfluid phase transition in a gas of Fermi atoms loaded on a three-dimensional optical lattice. When the lattice potential is strong, this system can be well described by an attractive Hubbard model. In this model, we calculate the superfluid phase transition temperature T_c, including both superfluid and (spin and charge) density fluctuations within the self-consistent t-matrix theory and fluctuation exchange approximation, respectively. Since we treat these fluctuations in a consistent manner, our theory satisfies the required particle-hole symmetry over the entire BCS–Bose-Einstein-condensation (BEC) crossover region. We show that charge density fluctuations compete against superfluid fluctuations near the half-filling, leading to the suppression of T_c. As a result, the maximum T_c is obtained away from the half-filling. Since the strong density fluctuations originate from the nesting property of the Fermi surface at the half-filling (which is absent in a uniform gas with no lattice potential), our results would be useful in considering lattice effects on strong-coupling superfluidity.

DOI: 10.1103/PhysRevA.77.063616 PACS number(s): 03.75.Ss, 71.10.Ca, 37.10.Jk

I. INTRODUCTION

An optical lattice is an artificial lattice produced by the standing wave of laser light [1]. In a cold atom gas loaded on an optical lattice, atoms feel a periodic potential due to the Stark effect. When the lattice potential is strong, this system can be well described by the Hubbard model, where atoms are hopping between nearest-neighbor sites, interacting with each other when they meet at the same lattice site. Since the Hubbard model is a fundamental model in condensed matter physics, it is expected that various topics discussed in this field may be solved by using the optical lattice system. Indeed, the superfluid-Mott insulator transition has been observed in a ^{87}Rb lattice Bose gas [2,3]. More recently, the superfluid state has been also realized in a ^{6}Li lattice Fermi gas [4,5].

Besides the optical lattice, a tunable interaction associated with a Feshbach resonance is also an advantage of cold atom gases [6,7]. Using this unique property, several experimental groups [8–11] have succeeded in realizing Fermi superfluids and the BCS–Bose-Einstein-condensation (BEC) crossover [12–19] in the absence of an optical lattice. The BCS-BEC crossover is a very interesting phenomenon, because one can study the weak-coupling BCS state and the BEC of tightly bound molecules in a unified manner by varying the strength of a pairing interaction. Since this tunable pairing interaction also works in an optical lattice, it is interesting to examine how the BCS-BEC crossover phenomenon is observed in the optical lattice system. We briefly note that, in the Hubbard model, interaction effects are parametrized by the scaled interaction U/t (where U and t represent an on-site pairing interaction and nearest-neighbor hopping, respectively). Thus, in addition to the direct tuning of the pairing interaction by a Feshbach resonance, continuous change from the weak- to strong-coupling regime can also be realized by adjusting the hopping parameter t by tuning the intensity of laser light producing the optical lattice.

The BCS-BEC crossover in the attractive Hubbard model has been discussed in superconductivity literature [20], in connection to strongly correlated electron systems. Nozières and Schmitt-Rink [13] pointed out that the mass enhancement of tightly bound molecules in the strong-coupling BEC regime is because of virtual dissociation of a bound molecule during hopping between lattice sites. This mass enhancement is expected to decrease the superfluid phase transition temperature T_c in the BEC regime, which has been theoretically confirmed by the self-consistent t-matrix theory [22], dynamical mean-field theory [23], and quantum Monte Carlo simulation [24]. Competition between pairing fluctuations and charge density wave (CDW) fluctuations [25] near the half-filling (which comes from the nesting property of the square-shape Fermi surface at the half-filling) has also been studied [26]. In two dimensions, Refs. [27,29] pointed out that this competition leads to vanishing T_c at the half-filling. For more details, we refer to Ref. [20].

In this paper, we investigate the superfluid phase transition in a gas of Fermi atoms loaded on a three-dimensional cubic optical lattice. Treating this system as the Hubbard model, we calculate T_c in the BCS-BEC crossover region, including pairing fluctuations, as well as CDW and spin density wave (SDW) fluctuations in a consistent manner within the self-consistent t-matrix approximation (SCTA) [16,17,30] and fluctuation exchange approximation (FLEX) [29], respectively. Our theory satisfies the required particle-hole symmetry over the entire BCS-BEC crossover region. While a finite T_c is obtained at the half-filling in contrast to the two-dimensional case [27], the superfluid phase transition is shown to be strongly influenced by CDW fluctuations near the half-filling. The resulting T_c takes the maximum value, not at the half-filling, but around the quarter-filling.

Since strong CDW fluctuations are characteristic of the lattice system we consider in this paper, the observation of the filling dependence of T_c would be an interesting problem.

This paper is organized as follows. In Sec. II, we explain our formulation. The self-consistent t-matrix approximation (SCTA) for pairing fluctuations and the fluctuation exchange approximation (FLEX) for CDW and SDW fluctuations are explained. In Sec. III, we present our numerical results for the superfluid phase transition temperature, only taking into account pairing fluctuations. We examine effects of CDW and SDW fluctuations on the superfluid phase transition in Sec. IV. Throughout this paper, we set $\hbar=k_B=1$.

II. FORMULATION

We consider a two-component Fermi gas in a three-dimensional cubic optical lattice. In superfluid Fermi gases, all the current experiments are using a broad Feshbach resonance [8–11]. In this case, details of the Feshbach resonance is known to not be important as far as we consider the interesting BCS-BEC crossover region, so that we can safely consider this system using the ordinary BCS model. In addition, as mentioned in the Introduction, a Fermi gas in an optical lattice can be well described by the Hubbard model when the lattice potential is strong. Under these conditions, we consider the attractive Hubbard model described by the Hamiltonian

$$H = -t\sum_{(i,j),\sigma}(c_{i,\sigma}^{\dagger}c_{j,\sigma}+\text{H.c.}) - U\sum_{i} n_{i\uparrow}n_{i\downarrow} - \mu\sum_{i,\sigma} n_{i,\sigma}. \quad (1)$$

Here, $c_{j,\sigma}$ is the annihilation operator of a Fermi atom at the jth lattice site, where the pseudospin $\sigma=\uparrow,\downarrow$ describes two atomic hyperfine states. t is the hopping matrix element between nearest-neighbor sites, and the summation (i,j) in the first term is taken over nearest-neighbor pairs. $n_{i\sigma}=c_{i\sigma}^{\dagger}c_{i\sigma}$ is the number operator. The on-site pairing interaction $-U$ (<0) is implicitly assumed to be tunable by using a Feshbach resonance. μ is the Fermi chemical potential. In Eq. (1), we have neglected effects of a harmonic trap, for simplicity.

We calculate the superfluid phase transition temperature T_c, extending SCTA developed by Haussmann [16,17] so as to include CDW and SDW fluctuations within the FLEX. Effects of these fluctuations are described by the self-energy $\Sigma(\boldsymbol{k},i\omega_m)$ in the single-particle Green's function $G(\boldsymbol{k},i\omega_m)$,

$$G(\boldsymbol{k},i\omega_m) = \frac{1}{i\omega_m - \varepsilon_{\boldsymbol{k}} + \mu - \Sigma(\boldsymbol{k},i\omega_m)}, \quad (2)$$

where $\varepsilon_{\boldsymbol{k}}\equiv -2t[\cos k_x+\cos k_y+\cos k_z]-\mu$ is the kinetic energy of a Fermi atom measured from the chemical potential μ (where the lattice constant is taken to be unity). ω_m is the fermion Matsubara frequency.

Figure 1(a) shows the self-energy correction coming from pairing fluctuations $(\equiv\Sigma_{\text{pp}})$. Summing up this type of diagrams within SCTA, we obtain

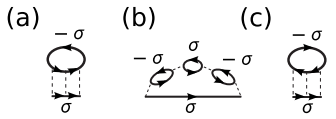

FIG. 1. Self-energy corrections describing (a) pairing fluctuations, (b) CDW fluctuations and SDW fluctuations of the z component, and (c) SDW fluctuations of the x and y components. The solid line and dashed line describe the single-particle Green's function G and the attractive interaction $-U$, respectively.

$$\Sigma_{\text{pp}}(\boldsymbol{k},i\omega_m) = \frac{1}{\beta}\sum_{\boldsymbol{q},i\nu_n}\Gamma_{\text{pp}}(\boldsymbol{q},i\nu_n)G(\boldsymbol{q}-\boldsymbol{k},i\nu_n-i\omega_m), \quad (3)$$

where ν_n is the boson Matsubara frequency. Hereafter, the factor $1/N$ of the lattice site number in front of momentum summation is abbreviated for simple presentation. Γ_{pp} is the particle-particle scattering vertex diagrammatically described by Fig. 2(a). The result is

$$\Gamma_{\text{pp}}(\boldsymbol{q},i\nu_n) = -\frac{U}{1-U\Pi_{\text{pp}}(\boldsymbol{q},i\nu_n)}, \quad (4)$$

where

$$\Pi_{\text{pp}}(\boldsymbol{q},i\nu_n) = \frac{1}{\beta}\sum_{\boldsymbol{k},i\omega_m} G(\boldsymbol{k},i\omega_m)G(\boldsymbol{q}-\boldsymbol{k},i\nu_n-i\omega_m) \quad (5)$$

is a correlation function describing fluctuations in the Cooper channel.

In Fig. 1, panels 1(b) and 1(c) describe fluctuations in the particle-hole channel within the FLEX. Figure 1(b) involves both CDW fluctuations and longitudinal SDW fluctuations. Figure 1(c) involves transverse SDW fluctuations. Summing up these diagrams, we obtain the self-energy corrections associated with CDW fluctuations $(\equiv\Sigma_{\text{ph}}^{\text{d}})$ and SDW fluctuations $(\equiv\Sigma_{\text{ph}}^{\text{s}})$ as

$$\begin{aligned}\Sigma_{\text{ph}}^{\text{d,s}}(\boldsymbol{k},i\omega_m) &= -\frac{U}{\beta}\sum_{\boldsymbol{q},i\nu_n}\Pi_{\text{ph}}(\boldsymbol{q},i\nu_n)\Gamma_{\text{ph}}^{\text{d,s}}(\boldsymbol{q},i\nu_n)\\ &\quad\times G(\boldsymbol{k}-\boldsymbol{q},i\omega_m-i\nu_n)\\ &\equiv \frac{1}{\beta}\sum_{\boldsymbol{q},i\nu_n} V_{\text{ph}}^{\text{d,s}}(\boldsymbol{q},i\nu_n)G(\boldsymbol{k}-\boldsymbol{q},i\omega_m-i\nu_n), \quad (6)\end{aligned}$$

where $V_{\text{ph}}^{\text{d,s}}$ is introduced for saving the computational time by performing the fast Fourier transformation (FFT), which

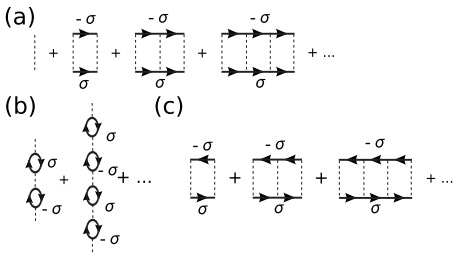

FIG. 2. Vertex functions of (a) particle-particle channel Γ_{pp} and (b),(c) particle-hole channel $\Gamma_{\text{ph}}^{\text{s,d}}$. In our calculation, the lowest order term in terms of U is included in Γ_{pp}.

is explained in Sec. III. Here, the vertex functions Γ^{d}_{ph} and Γ^{s}_{ph} are obtained from the sum of the diagrams shown in Figs. 2(a) and 2(b), and their expressions are given by

$$\Gamma^{d}_{ph}(\boldsymbol{q},i\nu_n) = -\frac{1}{2}\frac{U^2\Pi_{ph}(\boldsymbol{q},i\nu_n)}{1-U\Pi_{ph}(\boldsymbol{q},i\nu_n)}, \tag{7}$$

$$\Gamma^{s}_{ph}(\boldsymbol{q},i\nu_n) = \frac{3}{2}\frac{U^2\Pi_{ph}(\boldsymbol{q},i\nu_n)}{1+U\Pi_{ph}(\boldsymbol{q},i\nu_n)}. \tag{8}$$

In Eqs. (7) and (8), the correlation function $\Pi_{ph}(\boldsymbol{k},i\nu_n)$ describes fluctuations in the particle-hole channel, having the form

$$\Pi_{ph}(\boldsymbol{q},i\nu_n) = -\frac{1}{\beta}\sum_{\boldsymbol{k},i\omega_m} G(\boldsymbol{k},i\omega_m)G(\boldsymbol{k}-\boldsymbol{q},i\omega_m - i\nu_n). \tag{9}$$

The superfluid phase transition temperature T_c is determined from the Thouless criterion [16,17], stating that the superfluid phase transition occurs when the particle-particle scattering vertex $\Gamma_{pp}(\boldsymbol{q},i\nu_n)$ has a pole at $\boldsymbol{q}=\nu_n=0$. Using this, we obtain the equation for T_c as

$$1 = U\Pi_{pp}(\boldsymbol{q}=0,i\nu_n=0). \tag{10}$$

We note that Eq. (10) is affected by CDW and SDW fluctuations through the self-energy $\Sigma=\Sigma_{pp}+\Sigma^{d}_{ph}+\Sigma^{s}_{ph}$ in the Green's function.

In the weak-coupling BCS regime, we may set $\mu=\varepsilon_F$ (where ε_F is the Fermi energy) in Eq. (10). However, the chemical potential is known to deviate from ε_F, as one approaches the strong-coupling BEC regime [12,13]. This strong-coupling effect is taken into account by considering the equation for the filling number n (which gives the number of atoms per lattice site), given by

$$n = \frac{2}{\beta}\sum_{\boldsymbol{k},i\omega_m} e^{i\omega_m\delta}G(\boldsymbol{k},i\omega_m), \tag{11}$$

where δ is an infinitesimal positive number. We solve the coupled equations (10) and (11) to determine T_c and μ self-consistently for a given U and n.

At the half-filling $n=1$, the superfluid state and CDW are degenerate in the sense that they have the same phase transition temperature [20,26]. The CDW phase transition is characterized by the divergence of the charge susceptibility $\chi_{CDW}(\boldsymbol{Q})$ with the momentum $\boldsymbol{Q}=(\pi,\pi,\pi)$. In the random phase approximation, χ_{CDW} is given by

$$\chi_{CDW}(\boldsymbol{Q}=(\pi,\pi,\pi)) = \frac{1}{2}\frac{\Pi_{ph}(\boldsymbol{Q},0)}{1-U\Pi_{ph}(\boldsymbol{Q},0)}, \tag{12}$$

where the correlation function $\Pi_{ph}(\boldsymbol{Q},i\nu_n)$ is given by Eq. (9). Comparing Eq. (12) with Eq. (7), we find that the CDW vertex function $\Gamma^{d}_{ph}(\boldsymbol{Q},i\nu_n=0)$ also diverges at T_c. This CDW instability at the superfluid phase transition temperature T_c is absent when $n\neq 1$ due to the absence of the perfect nesting of the Fermi surface. However, since the denominator $1-U\Pi_{ph}(\boldsymbol{Q},i\nu_n=0)$ in Eq. (12) is still small at T_c near the half-filling, strong CDW fluctuations are expected when $n\sim 1$.

In contrast, the SDW vertex function Γ^{s}_{ph} in Eq. (8) does not diverge at T_c even when $n=1$. Namely, spin fluctuations are weak in the attractive Hubbard model.

III. EFFECTS OF PAIRING FLUCTUATIONS ON T_c AND μ IN THE BCS-BEC CROSSOVER REGION

In the following two sections, we show our numerical results obtained by solving the coupled equations (10) and (11). In this section, we first consider T_c in the BCS-BEC crossover, including pairing fluctuations only. Although one cannot actually ignore strong CDW fluctuations near the half-filling, examining this simple case is still useful in considering the importance of CDW and SDW fluctuations. We separately discuss effects of CDW and SDW fluctuations in Sec. IV.

Before showing our results, we summarize the outline of computation. In solving the coupled equations (10) and (11), we use the fact that the self-energy $\Sigma=\Sigma_{pp}+\Sigma^{d}_{ph}+\Sigma^{s}_{ph}$ in Eqs. (3) and (6), the correlation functions Π_{pp} and Π_{ph} in Eqs. (5) and (9), and the number equation in Eq. (11) have simple expressions in real space, as

$$\begin{aligned}\Sigma(\boldsymbol{r},\tau) &= \Sigma_{pp}(\boldsymbol{r},\tau)+\Sigma^{d}_{ph}(\boldsymbol{r},\tau)+\Sigma^{s}_{ph}(\boldsymbol{r},\tau)\\ &= \Gamma_{pp}(\boldsymbol{r},\tau)G(-\boldsymbol{r},-\tau)+[V^{d}_{ph}(\boldsymbol{r},\tau)+V^{s}_{ph}(\boldsymbol{r},\tau)]G(\boldsymbol{r},\tau),\end{aligned} \tag{13}$$

$$\Pi_{pp}(\boldsymbol{r},\tau) = G(\boldsymbol{r},\tau)G(\boldsymbol{r},\tau), \tag{14}$$

$$\Pi_{ph}(\boldsymbol{r},\tau) = -G(\boldsymbol{r},\tau)G(-\boldsymbol{r},-\tau), \tag{15}$$

$$n = 2G(\boldsymbol{r}=0,\tau=-\delta). \tag{16}$$

Here, $\boldsymbol{r}$ is the spatial position of a lattice site and τ is the imaginary time. The Fourier transformation is defined by

$$G(\boldsymbol{r},\tau) = \frac{1}{\beta}\sum_{\boldsymbol{k},i\omega_m} G(\boldsymbol{k},i\omega_m)e^{i(\boldsymbol{k}\cdot\boldsymbol{r}-\omega_m\tau)},$$

$$G(\boldsymbol{k},i\omega_m) = \sum_{\boldsymbol{r}}\int_0^\beta d\tau G(\boldsymbol{k},\tau)e^{-i(\boldsymbol{k}\cdot\boldsymbol{r}-\omega_m\tau)}. \tag{17}$$

To use Eqs. (13)–(16), we employ the FFT method [31]. We discretize the momentum region $0\le k_x,k_y,k_z\le\pi$ into $16\times16\times16$ cells. For the frequency summations, we introduce a finite cutoff frequency $\omega_{max}=\pi T(2n_{max}+1)$ for fermions and $\nu_{max}=2\pi Tn_{max}$ for bosons, with $n_{max}=512$. The values of these cutoffs are chosen so as to be much larger than the bandwidth $2zt$ (where $z=6$ is the coordination number of the simple cubic lattice), as well as the magnitude of the pairing interaction U. To avoid effects of these cutoff frequencies, we use the method discussed in [29]. We explain the outline of this method in the Appendix.

In the numerical calculations, we start from a high temperature region ($T\gg T_c$), where the denominator of $\Gamma_{pp}(\boldsymbol{q}=0,i\nu_n=0)$ in Eq. (4), $1-U\Pi_{pp}(\boldsymbol{q}=0,i\nu_n=0)$, does not take an unphysical negative value, and then slowly approach the low temperature region to look for T_c. Since $\Gamma_{pp}(\boldsymbol{q}=\boldsymbol{0},i\nu_n$

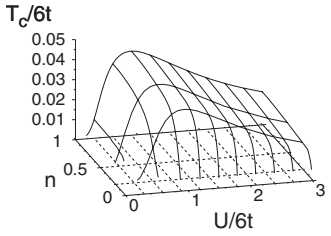

FIG. 3. Superfluid phase transition temperature T_c as a function of pairing interaction U and filling number n. In this figure, and in Fig. 4, we only include pairing fluctuations described by Σ_{pp}. Since T_c at the filling $2-n$ is the same as T_c at n due to the particle-hole symmetry, we only show the result less than half-filling ($n \leq 1$).

$=0$) diverges at T_c [note that $\Gamma^{d}_{ph}(\boldsymbol{q}=\boldsymbol{Q}, i\nu_n=0)$ also diverges at T_c when $n=1$], we need to avoid this singularity in numerically executing the summation in Eq. (3) and also in calculating Eq. (6) when $n=1$. We note that these summations should converge in the three-dimensional system we are considering in the present paper.

Figure 3 shows the calculated T_c in the BCS-BEC crossover. In this calculation, we only include the self-energy Σ_{pp} associated with pairing fluctuations. Since the Hubbard model has the particle-hole symmetry, the filling dependence of T_c is symmetric with respect to $n=1$ (although we do not show it explicitly). Namely, for a given U, Fig. 3 shows that the maximum T_c is obtained at the half-filling $n=1$, while T_c vanishes at $n=2$ as in the case of $n=0$.

In the weak-coupling BCS regime ($U/6t \lesssim 1$), T_c is an increasing function of U. This behavior agrees with the well-known mean-field BCS result,

$$T_c \propto te^{-1/N(0)U}, \tag{18}$$

where $N(0)$ is the density of states at the Fermi level. In this regime, since T_c is comparable to the binding energy E_{bind} of a Cooper pair at $T=0$, the increase of T_c reflects the enhancement of E_{bind} as one approaches the strong-coupling regime.

For a given filling number n, the maximum T_c ($\equiv T_c^{max}$) is obtained around the intermediate coupling region $U/6t \sim 1$. At the half-filling ($n=1$), we obtain $T_c^{max}=0.042$ at $U/6t=0.9$. T_c then decreases as one further increases the magnitude of U. The decrease of T_c in the BEC regime is characteristic of the BCS-BEC crossover in the Hubbard model [20]. In a uniform Fermi gas with no lattice potential, T_c approaches the constant value $T_c=0.218\varepsilon_F$ in the BEC limit [15,16,18].

We note that the decrease of T_c in the BEC regime does not mean the small binding energy of a bound molecule in this regime. As shown in Fig. 4, while the chemical potential μ is almost equal to the Fermi energy ε_F at $U=0$ (apart from the weak temperature effect), it becomes smaller than the bottom of the band ($=-6t$) in the strong coupling regime. This means the existence of a *finite energy gap* $E_g=|\mu|-6t$ in the Fermi single-particle excitations in the BEC regime. Since E_g is directly related to the dissociation energy of a bound molecule, we find that the binding energy E_b continues to increase even in the BEC regime (although T_c decreases as shown in Fig. 3).

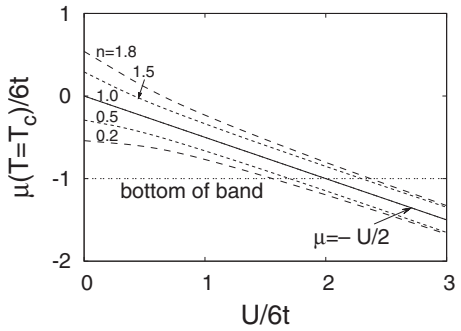

FIG. 4. Chemical potential μ as a function of U at T_c. $\mu=-U/2$ is the exact solution at the half-filling $n=1$. At $U=0$, apart from the weak temperature effect, μ is almost equal to the Fermi energy ε_F for a given filling number n.

To understand the physics behind the decreasing T_c in the BEC regime, it is helpful to derive an effective model valid for this regime. To do this, we note that in the BEC regime, tightly bound molecules already have been formed above T_c. In this case, as pointed out in Ref. [13], molecular motion is accompanied by virtual dissociation, because each atom in a molecule has to move one by one in the Hubbard model. In addition, this virtual dissociation also leads to a repulsive interaction between molecules [13]. Including these effects within the second-order perturbation in terms of the hopping t, we obtain the effective Hamiltonian [21]

$$H_{eff} = -\frac{2t^2}{U}\sum_{(i,j)}[b_i^\dagger b_j + \text{H.c.}] + \frac{4t^2}{U}\sum_{(i,j)} n_i^B n_j^B - \mu_B \sum_i n_i^B, \tag{19}$$

where $b_i^\dagger = c_{i\uparrow}^\dagger c_{i\downarrow}^\dagger$ describes a molecule at the ith lattice site, and $n_i^B = (n_{i\uparrow}+n_{i\downarrow})/2$ gives the number of molecules under the assumption that all the atoms form small on-site bound pairs. $\mu_B = 2\mu + U + 2zt^2/U$ is the molecular chemical potential to control the molecular density. In Eq. (19), double occupancy of molecules is forbidden due to the Pauli's exclusion principle of Fermi atoms in them. Noting this and commutation relations, $[b_i^\dagger, b_i] = 2(n_i^B - 1/2)$, $[n_i^B - 1/2, b_i^\dagger] = b_i^\dagger$, and $[n_i^B - 1/2, b_i] = -b_i$, we can map Eq. (15) onto the $S=1/2$ Heisenberg model, by replacing $(b_i^\dagger, b_i, n_i^B - 1/2)$ with $[(-1)^i S_i^+, (-1)^i S_i^-, S_i^z]$,

$$H_{eff} = J\sum_{(i,j)} \mathbf{S}_i \cdot \mathbf{S}_j - h_B \sum_i S_i^z. \tag{20}$$

Here, $J = 4t^2/U$ is an exchange interaction and $h_B = \mu_B - 2zt^2/U$ works as an external magnetic field. Since the $S_i^z = -1/2$ and $S_i^z = +1/2$ states in Eq. (16), respectively, correspond to vacant and occupied sites in the effective model in Eq. (19), the half-filling case is described by setting $h_B = 0$ in Eq. (20). Equation (20) clearly shows that the "Néel temperature T_N" (which corresponds to T_c in the original Hubbard model) is lower for larger U, consistent with the decreasing T_c in the strong-coupling BEC regime shown in Fig. 3.

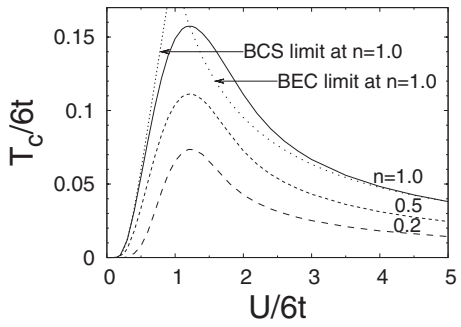

FIG. 5. Calculated T_c within the NSR theory. "BCS limit" is the mean-field BCS result with $\mu=\varepsilon_F$. "BEC limit" shows the T_c of an ideal molecular Bose gas.

The Néel temperature of the Heisenberg model has been studied by various methods. It has been shown that the mean-field result $T_N=6t^2/U$ is suppressed by spin fluctuations to be $T_N=3.59t^2/U$ (high temperature expansion) [32] and $T_N=3.78t^2/U$ (quantum Monte Carlo method) [33]. In the present calculation, we obtain $T_c\simeq 1.5t^2/U<(3.59\sim 3.78)t^2/U$ in the BEC regime, showing that the present calculation based on the SCTA underestimates T_c in the BEC regime.

One reason for this discrepancy is the approximate treatment of the interaction between molecules. To see this, we consider the BCS-BEC crossover problem within the Gaussian fluctuation theory developed by Nozières and Schmitt-Rink [13]. (We refer to this theory as the NSR theory in the following.) In the NSR theory, one also solves the coupled equations (10) and (11), where the single-particle Green's function G and the correlation function Π_{pp} are now replaced by

$$G(\boldsymbol{p},i\omega_m)=G_0(\boldsymbol{k},i\omega_m)+G_0(\boldsymbol{k},i\omega_m)\Sigma_{pp}(\boldsymbol{k},i\omega_m)G_0(\boldsymbol{k},i\omega_m), \tag{21}$$

$$\Pi_{pp}(\boldsymbol{q},i\nu_n)=\frac{1}{\beta}\sum_{\boldsymbol{k},i\omega_m} G_0(\boldsymbol{k},i\omega_m)G_0(\boldsymbol{q}-\boldsymbol{k},i\nu_n-i\omega_m), \tag{22}$$

where $G_0(\boldsymbol{k},i\omega_m)^{-1}=i\omega_m-\varepsilon_k+\mu$ is the Green's function in a free Fermi gas. The self-energy part in Eq. (21) is given by

$$\Sigma_{pp}(\boldsymbol{k},i\omega_m)=\frac{1}{\beta}\sum_{\boldsymbol{q},i\nu_n}\Gamma_{pp}(\boldsymbol{q},i\nu_n)G_0(\boldsymbol{q}-\boldsymbol{k},i\nu_n-i\omega_m). \tag{23}$$

The particle-particle scattering vertex Γ_{pp} is given by Eq. (4), where Π_{pp} is replaced by Eq. (22).

Figure 5 shows the calculated T_c based on the NSR theory. Comparing this result with Fig. 3, we find that the NSR theory gives higher T_c. Since the NSR theory is a low density approximation [13] [note that only the free propagator G_0 is used and the self-energy correction is only taken into account to the first order in the number equation (10)], the difference between the two is more remarkable in higher filling cases.

In the BEC limit of the NSR theory, Eq. (10) gives $\mu=-U/2$, and the number equation (11) reduces to the condition for a BEC in an ideal Bose gas,

$$\frac{n}{2}=\sum_{\boldsymbol{q}}\frac{1}{e^{\beta(E_{\boldsymbol{q}}^B-\bar{\mu}_B)}-1}, \tag{24}$$

where $E_{\boldsymbol{q}}^B=-2(2t^2/U)[\cos q_x+\cos q_y+\cos q_z]$ and $\bar{\mu}_B=-6(2t^2/U)$. Indeed, Fig. 5 shows that T_c obtained from Eq. (24) well describes the NSR result in the strong-coupling regime. Noting that the kinetic energy $E_{\boldsymbol{q}}^B$ can be also obtained from the first term in Eq. (19) when one regards b_i as a boson operator, we find that the NSR theory ignores the repulsive interaction between molecules given by the second term in Eq. (19).

In a uniform Fermi gas with no lattice potential, Haussmann pointed out that, in the BEC regime, the SCTA includes the interaction between molecules within the Born approximation [16]. This molecular interaction can be written as $U_B=4\pi a_B/M_B$, where M_B is a molecular mass. The s-wave molecular scattering length a_B is related to the s-wave atomic scattering length a_s as $a_B=2a_s$. Even in the presence of the lattice, the molecular interaction is expected to be included within the same approximation level. Thus, we find that the lower T_c within SCTA than the NSR result originates from the molecular interaction. Namely, the molecular interaction lowers T_c in the BEC regime in the lattice system.

Recent work [34–37] on a uniform Fermi gas has clarified that, when one carefully treats higher order molecular scattering processes and a finite value of molecular binding energy, a_B reduces to $a_B=0.6a_s<2a_s$. This clearly indicates an *overestimate* of the magnitude of molecular interaction in the SCTA. When we apply this discussion to the present lattice system, one reason for the underestimate of T_c $[=1.5t^2/U<(3.59\text{–}3.78)t^2/U]$ is expected to be the overestimate of the molecular interaction. When one could correct this point, T_c would be higher to be close to the "Néel temperature" of the Heisenberg model in Eq. (20). This improvement is an interesting problem; however, in this paper, leaving this as a future problem, we treat pairing fluctuations within the SCTA and discuss effects of CDW and SDW fluctuations in the next section.

Before ending this section, we briefly note that the NSR theory does not satisfy the particle-hole symmetry, when it is applied to the Hubbard model. As shown in Fig. 6, the calculated T_c based on the NSR theory is unphysical around $n=2$ (note that the system must be a band insulator at $n=2$, leading to vanishing T_c). We also find that the required symmetric filling dependence of T_c with respect to $n=1$ is not obtained within the NSR theory. In addition, although the chemical potential must satisfy $\mu=-U/2$ at $n=1$ due to the particle-hole symmetry [38], the NSR result satisfies it only in the BEC limit $U\to\infty$, as shown in Fig. 7. In contrast, in addition to the symmetric filling dependence of T_c, the SCTA can also reproduce the exact result $\mu=-U/2$ at $n=1$ over the entire BCS-BEC crossover. (See Fig. 4.) We emphasize that satisfying these required conditions is important in any consistent theory.

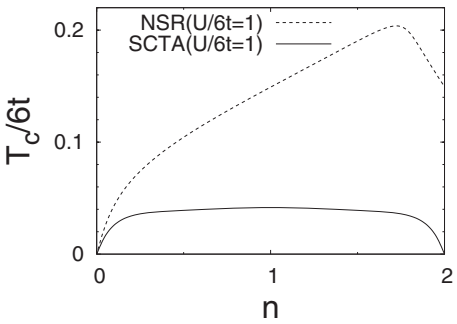

FIG. 6. T_c as a function of the filling number n. The result within the SCTA and that within the NSR theory are compared. We set $U/6t=1$.

IV. EFFECTS OF CDW AND SDW FLUCTUATIONS

Figures 8 and 9 show calculated T_c and $\mu(T_c)$, respectively, in the BCS-BEC crossover, when the CDW (Σ_{ph}^{d}) and SDW (Σ_{ph}^{s}) fluctuations are both taken into account. As shown in Fig. 9, the required condition $\mu=-U/2$ at $n=1$ is still satisfied when one includes CDW and SDW fluctuations within the FLEX.

Comparing Fig. 4 with Fig. 9, one finds that effects of CDW and SDW fluctuations on the chemical potential μ are weak. In contrast, from the comparison of Fig. 3 and Fig. 8, T_c is found to be suppressed near the half-filling when these fluctuations are taken into account. We note that the suppression of T_c near the half-filling also has been obtained by using the Monte Carlo simulation [24,28].

To see the suppression of T_c more clearly, we show T_c at $n=1$ in Fig. 10. At the half-filling, the CDW instability occurs simultaneously [which is confirmed by the vanishing denominator of the charge susceptibility $\chi(\boldsymbol{Q})$ as shown in Fig. 11], leading to the remarkable suppression of T_c. However, in contrast to the two-dimensional case where T_c vanishes at $n=1$ [27], we still obtain a finite T_c even at the half-filling. Since strong CDW fluctuations would decrease the density of states near the Fermi level as the pseudogap effects by pairing fluctuations, we expect that this effect is an origin of the suppression of T_c near $n=1$. To confirm this mechanism, we need the analytically continued Green's function to calculate single-particle excitations. We will discuss this problem elsewhere.

Although SDW fluctuations are weak in the attractive Hubbard model, we still find their effects around $U/6t\sim 1$ in Fig. 10. From the comparison of the result referred to as "SCTA+CDW+SDW" with "SCTA+CDW" in Fig. 10, we find that SDW fluctuations weaken the suppression of T_c by CDW fluctuations.

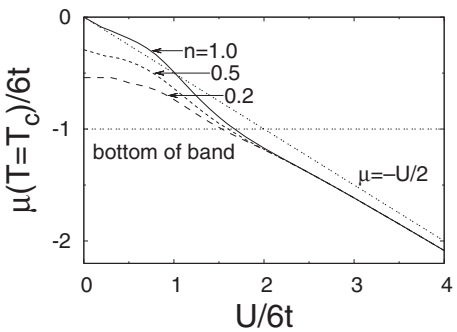

FIG. 7. Chemical potential μ at T_c calculated within the NSR theory.

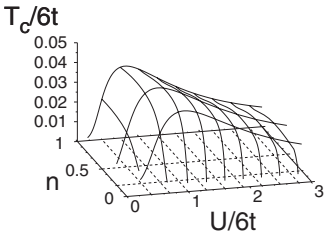

FIG. 8. Superfluid phase transition temperature T_c as a function of pairing interaction U and filling number n. In this figure, and in Fig. 9, we include CDW and SDW fluctuations described by $\Sigma_{ph}^{d,s}$ in addition to pairing fluctuations. In comparison with Fig. 4, T_c around $n=1$ are suppressed in the strong-coupling regime.

In this intermediate coupling regime, since the binding energy of a Cooper pair is not very strong, (pseudo)spin degrees of freedom still remain, which contribute to SDW fluctuations. As one approaches the strong-coupling regime, these spin degrees from freedom disappear due to the formation of singlet pairs. Indeed, in Fig. 10, the two results, "SCTA+CDW+SDW" and "SCTA+CDW," give almost the same T_c when $U/6t\gtrsim 3$.

Although the degeneracy of the superfluid state and CDW is absent when $n\neq 1$, we can still expect strong influence of CDW near the half-filling due to strong enhancement of charge susceptibility shown in Fig. 11. Indeed, as shown in Fig. 12, CDW fluctuations suppress T_c near $n=1$. (Compare "SCTA" with "SCTA+CDW+SDW" in Fig. 12.) The maximum T_c is thus obtained, not at the half-filling, but away from the half-filling. Although SDW fluctuations enhance T_c, the overall behavior is unchanged. (Compare "SCTA+CDW+SDW" with "SCTA+CDW" in Fig. 12.) Since spin degrees of freedom are almost absent in the strong-coupling regime, effects of SDW fluctuations are weaker in the lower panel (BEC regime) than the upper panel (BCS-crossover regime) in Fig. 12.

V. SUMMARY

To summarize, we have discussed the superfluid phase transition in the BCS-BEC crossover regime of a two-

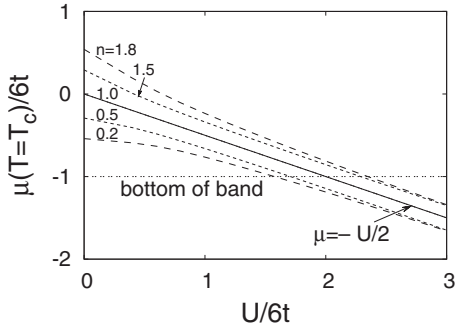

FIG. 9. Chemical potential μ as a function of U at T_c when we consider CDW and SDW fluctuations in addition to pairing fluctuations. Self-consistent treatment of CDW and SDW fluctuations does not break the particle-hole symmetry condition $\mu=-U/2$ at $n=1$.

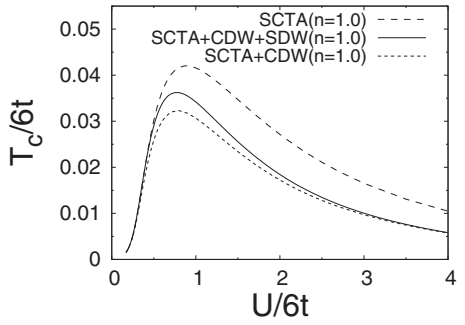

FIG. 10. Effects of CDW and SDW fluctuations on T_c at the half-filling $n=1$. SCTA: Pairing fluctuations only are included. SCTA+CDW+SDW: Pairing, CDW, and SDW fluctuations are all included. SCTA+CDW: Pairing and CDW fluctuations are taken into account. These abbreviations are also used in Figs. 11 and 12.

component Fermi gas loaded on a three-dimensional optical lattice. Treating this system as the attractive Hubbard model, we calculated the superfluid phase transition temperature T_c, including pairing fluctuations within the self-consistent t-matrix theory, as well as CDW and SDW fluctuations within the fluctuation exchange approximation. We determined T_c and the Fermi chemical potential μ self-consistently as functions of the pairing interaction U and filling number n in the BCS-BEC crossover region, by solving the equation for T_c, together with the number equation.

CDW fluctuations are strong near the half-filling due to the nesting property of the Fermi surface at $n=1$. These strong fluctuations remarkably decrease the superfluid phase transition temperature T_c around $n=1$. As a result, the maximum T_c is obtained, not at the half-filling, but away from the half-filling. We also showed that, although SDW fluctuations are weak in the attractive Hubbard model, they cause T_c to increase slightly in the intermediate coupling region $U/6t \sim 1$.

We have also discussed the validity of the SCTA. Our theory satisfies the required condition associated with the particle-hole symmetry of the Hubbard model which is not derived from NSR theory. Therefore, it would be a good starting point to improve the BCS-BEC crossover theory in optical lattices. On the other hand, we showed that this approximation underestimates T_c in the BEC regime. As a key to understand this, we pointed out the importance of a repulsive interaction between molecules. Since the Gaussian fluctuation theory (which completely ignores the molecular interaction at T_c) largely *overestimates* T_c, we expect that the SCTA overestimates effects of the molecular interaction. Indeed, the overestimate of the molecule interaction within the SCTA has been pointed out [16,34–37] in a uniform Fermi gas with no lattice potential. Inclusion of the correct value of the molecular interaction in the present theory is our future problem.

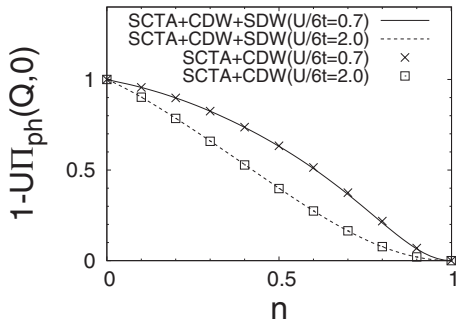

FIG. 11. Denominator of the static charge susceptibility $\chi(\boldsymbol{Q})$ in Eq. (12) at the superfluid phase transition temperature T_c. The CDW instability is determined when $1-U\Pi_{ph}(\boldsymbol{q}=\boldsymbol{Q},\omega=0)=0$ is realized.

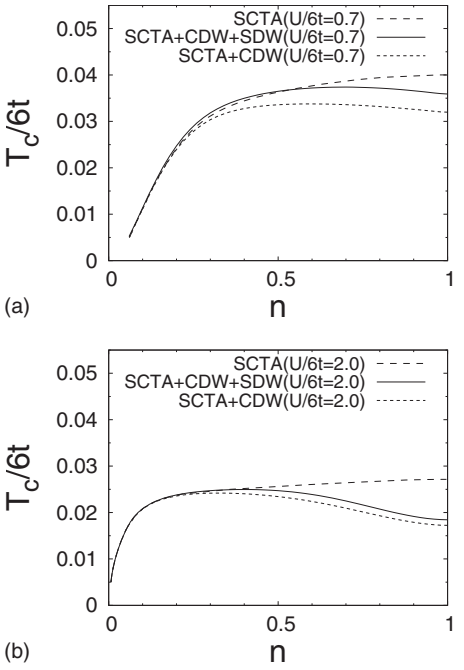

FIG. 12. Filling dependence of the superfluid transition temperature T_c. Upper and lower panels show the cases of the weak-coupling BCS regime ($U/6t=0.7$) and strong-coupling BEC regime ($U/6t=2$), respectively.

So far, the superfluid Fermi gas in an optical lattice has been realized when the lattice potential is weak [4]. To realize the system describable by the Hubbard model in a cold gas of Fermi atoms, one needs to use a stronger optical lattice potential in order that the two assumptions in the Hubbard model, i.e., including only the nearest-neighbor hopping and neglecting higher bands, can be justified. However, such a stronger lattice potential also leads to a lower T_c because of the small value of hopping parameter t. To realize Fermi superfluids in such a difficult situation, our results indicate that the filling number should be set to be away from the half-filling $n=1$ (to avoid the suppression of T_c by CDW fluctuations) so that one can reach T_c as easy as possible under a given experimental condition. Since the Hubbard model is a fundamental model in condensed matter physics, realization of Fermi superfluid in the Hubbard model produced by strong optical lattice potential would be a great challenge in cold atom physics.

ACKNOWLEDGMENTS

This work was supported by a Grant-in-Aid for Scientific

Research of Priority Area "Physics of New Quantum Phase in Superclean Materials" from the Ministry of Education, Culture, Sports, Science and Technology of Japan (MEXT). The authors were also supported by (MEXT) Contracts No. 19340099 (H.T. and K.M.) and No. 19540420 (Y.O.).

APPENDIX: APPLICATION OF FFT TO FREQUENCY SUMMATIONS

In this appendix, we explain how to use the FFT algorithm in transforming between the Matsubara frequency and the imaginary time. As an example, we consider the single-particle Green's function G here. However, the method explained in this appendix can be used also in calculating the self-energies as well as correlation functions.

We introduce a Matsubara frequency cutoff $\omega_{\max}=\pi T(2n_{\max}+1)$ and evaluate the Green's function by using the Fourier transformation. By introducing this cutoff frequency, the Fourier transformation from the Matsubara frequency into imaginary time can be rewritten as (suppressing the variables $\boldsymbol{k}$ and $\boldsymbol{r}$),

$$G(\tau)=T\sum_{m=-n_{\max}-1}^{n_{\max}} G(i\omega_m)e^{-i\omega_m\tau}$$
$$=2T\sum_{m=0}^{n_{\max}}\{\mathrm{Re}[G(i\omega_m)]\cos\omega_m\tau+\mathrm{Im}[G(i\omega_m)]\sin\omega_m\tau\}, \tag{A1}$$

where we have used the analytic property $G(-i\omega_m)=G^*(i\omega_m)$, as well as the fact that $G(\tau)$ is a real function. Replacing τ by $\beta-\tau$ in Eq. (A1), we have

$$G(\beta-\tau)=2T\sum_{m=0}^{n_{\max}}\{-\mathrm{Re}[G(i\omega_m)]\cos\omega_m\tau$$
$$+\mathrm{Im}[G(i\omega_m)]\sin\omega_m\tau\}. \tag{A2}$$

Thus, one may only consider the region $0\le\tau<\beta/2$ in executing the cosine (sine) Fourier transformation from the Matsubara frequency into imaginary time. In numerical calculations, we divide the region $0\le\tau<\beta/2$ into $n_{\max}$ cells and use the FFT method.

When we calculate the inverse Fourier transformation, we meet the problem that the expected high-frequency behavior $G(\boldsymbol{k},i\omega_m)\sim 1/i\omega_m$ is not obtained because of the introduced cutoff frequency $\omega_{\max}$. To avoid this problem, we rewrite the inverse Fourier transformation in the form

$$G(i\omega_m)=\int_0^\beta d\tau G(\tau)e^{i\omega_m\tau}=\sum_{j=1}^{2n_{\max}}\int_{\tau_{j-1}}^{\tau_j} d\tau G(\tau)e^{i\omega_m\tau}. \tag{A3}$$

Here, $\tau_j=\Delta\tau j$, where $\Delta\tau=\beta/2n_{\max}$. When we approximately write the Green's function in the region $\tau=[\tau_{j-1},\tau_j]$ as $G(\tau)\simeq G(\tau_{j-1})+(\tau-\tau_{j-1})\times[G(\tau_j)-G(\tau_{j-1})]/\Delta\tau$, we can execute the integrals in Eq. (A3). The result is

$$G(i\omega_m)=\frac{1}{i\omega_m}[-G(\tau_{2n_{\max}}=\beta-\delta)-G(\tau_0=+\delta)]$$
$$+\frac{1}{\omega_m^2\Delta\tau}\Bigg(-\{G(\tau_1)-G(\tau_0)\}$$
$$+\sum_{j=1}^{2n_{\max}-1}\{2G(\tau_j)-G(\tau_{j+1})-G(\tau_{j-1})\}e^{i\omega_m\tau_j}$$
$$-\{G(\tau_{2n_{\max}})-G(\tau_{2n_{\max}-1})\}\Bigg), \tag{A4}$$

where δ is a infinitesimal positive number. In Eq. (A4), because $G(\beta-\delta)=-G(-\delta)$, the first term remains finite due to the discontinuity of the Green's function at $\tau=0$, giving the expected high frequency behavior $(\sim 1/i\omega_m)$. We apply the FFT to calculate the second term in Eq. (A4). We note that Eq. (A4) also has been derived in Ref. [29] by integration by parts.

[1] For a review, see L. Pitaevskii and S. Stringari, *Bose-Einstein Condensation* (Oxford University Press, New York, 2003), Chap. 16.
[2] M. Greiner, O. Mandel, T. Esslinger, T. W. Hänsch, and I. Bloch, Nature (London) **415**, 39 (2002).
[3] T. Stöferle, H. Moritz, C. Schori, M. Köhl, and T. Esslinger, Phys. Rev. Lett. **92**, 130403 (2004).
[4] J. K. Chin, D. E. Miller, Y. Liu, C. Stan, W. Setiawan, C. Sanner, K. Xu, and W. Ketterle, Nature (London) **443**, 961 (2006).
[5] D. E. Miller, J. K. Chin, C. A. Stan, Y. Liu, W. Setiawan, C. Sanner, and W. Ketterle, Phys. Rev. Lett. **99**, 070402 (2007).
[6] E. Timmermans, K. Furuya, P. W. Milonni, and A. K. Kerman, Phys. Lett. A **285**, 228 (2001).
[7] M. Holland, S. J. J. M. F. Kokkelmans, M. L. Chiofalo, and R. Walser, Phys. Rev. Lett. **87**, 120406 (2001).
[8] C. A. Regal, M. Greiner, and D. S. Jin, Phys. Rev. Lett. **92**, 040403 (2004).
[9] M. Bartenstein, A. Altmeyer, S. Riedl, S. Jochim, C. Chin, J. H. Denschlag, and R. Grimm, Phys. Rev. Lett. **92**, 120401 (2004).
[10] M. W. Zwierlein, C. A. Stan, C. H. Schunck, S. M. F. Raupach, A. J. Kerman, and W. Ketterle, Phys. Rev. Lett. **92**, 120403 (2004).
[11] J. Kinast, S. L. Hemmer, M. E. Gehm, A. Turlapov, and J. E. Thomas, Phys. Rev. Lett. **92**, 150402 (2004).
[12] A. J. Leggett, in *Modern Trend in the Theory of Condensed Matter*, edited by A. Pekalski and J. Przystawa (Springer-Verlag, Berlin, 1980), p. 14.
[13] P. Nozières and S. Schmitt-Rink, J. Low Temp. Phys. **59**, 195 (1985).
[14] A. Tokumitu, K. Miyake, and K. Yamada, Phys. Rev. B **47**,

11988 (1993).
[15] C. A. R. Sá de Melo, M. Randeria, and J. R. Engelbrecht, Phys. Rev. Lett. **71**, 3202 (1993).
[16] R. Haussmann, Phys. Rev. B **49**, 12975 (1994).
[17] R. Haussmann, *Self-Consistent Quantum-Field Theory and Bosonization for Strongly Correlated Electron Systems* (Springer-Verlag, Berlin, 1999), Chap. 3.
[18] Y. Ohashi and A. Griffin, Phys. Rev. Lett. **89**, 130402 (2002).
[19] For reviews, see Q. Chen, J. Stajic, S. Tan, and K. Levin, Phys. Rep. **412**, 1 (2005); S. Giorgini, L. Pitaevskii, and S. Stringari, e-print arXiv:cond-mat/07063360.
[20] For a review, see R. Micnas, J. Ranninger, and S. Robaszkiewicz, Rev. Mod. Phys. **62**, 113 (1990).
[21] S. Robaszkiewicz, R. Micnas, and K. A. Chao, Phys. Rev. B **23**, 1447 (1981).
[22] M. Keller, W. Metzner, and U. Schöllwock, Phys. Rev. B **60**, 3499 (1999).
[23] M. Keller, W. Metzner, and U. Schöllwock, Phys. Rev. Lett. **86**, 4612 (2001).
[24] A. Sewer, X. Zotos, and H. Beck, Phys. Rev. B **66**, 140504(R) (2002).
[25] In the present paper, we deal with a *neutral* Fermi gas. However, we use the term *charge* density wave (CDW) to describe density fluctuations, following the convention used in condensed matter physics.
[26] A. Taraphder, H. R. Krishnamurthy, Rahul Pandit, and T. V. Ramakrishnan, Phys. Rev. B **52**, 1368 (1995).
[27] R. T. Scalettar, E. Y. Loh, J. E. Gubernatis, A. Moreo, S. R. White, D. J. Scalapino, R. L. Sugar, and E. Dagotto, Phys. Rev. Lett. **62**, 1407 (1989).
[28] R. R. dos Santos, Phys. Rev. B **50**, 635 (1994).
[29] J. J. Deisz, D. W. Hess, and J. W. Serene, Phys. Rev. B **66**, 014539 (2002).
[30] J. R. Engelbrecht, H. Zhao, and A. Nazarenko, J. Phys. Chem. Solids **63**, 2237 (2002).
[31] Since the mean-field Green's function and the mean-field self-energy can be analytically obtained as $G_{\mathrm{HF}}^{-1}(\boldsymbol{k}, i\omega_m) = i\omega_m - \epsilon_{\boldsymbol{k}} + \mu - \Sigma_{\mathrm{HF}}$ and $\Sigma_{\mathrm{HF}} = -Un/2$, respectively, we only calculate their higher-order parts numerically by subtracting the mean-field parts. For the particle-particle vertex function Γ_{pp}, we apply the FFT from the second order in terms of the interaction U.
[32] G. S. Rushbrooke and P. J. Wood, Mol. Phys. **6**, 409 (1963).
[33] A. W. Sandvik, Phys. Rev. Lett. **80**, 5196 (1998).
[34] P. Pieri and G. C. Strinati, Phys. Rev. B **61**, 15370 (2000).
[35] D. S. Petrov, C. Salomon, and G. V. Shlyapnikov, Phys. Rev. Lett. **93**, 090404 (2004); Phys. Rev. A **71**, 012708 (2005).
[36] G. E. Astrakharchik, J. Boronat, J. Casulleras, and S. Giorgini, Phys. Rev. Lett. **93**, 200404 (2004).
[37] Y. Ohashi, J. Phys. Soc. Jpn. **74**, 2659 (2005).
[38] See, for example, S. G. Ovchinnikov and V. V. Val'kov, *Hubbard Operators in the Theory of Strongly Correlated Electrons* (Imperial College Press, London, 2004), Chap. 1.